INTERNATIONAL SOCIETY FOR SOIL MECHANICS AND GEOTECHNICAL ENGINEERING

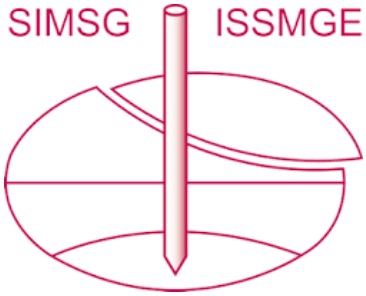

This paper was downloaded from the Online Library of the International Society for Soil Mechanics and Geotechnical Engineering (ISSMGE). The library is available here:

https://www.issmge.org/publications/online-library

This is an open-access database that archives thousands of papers published under the Auspices of the ISSMGE and maintained by the Innovation and Development Committee of ISSMGE.

The paper was published in the proceedings of the 20th International Conference on Soil Mechanics and Geotechnical Engineering and was edited by Mizanur Rahman and Mark Jaksa. The conference was held from May 1st to May 5th 2022 in Sydney, Australia.

Proceedings of the 20th International Conference on Soil Mechanics and Geotechnical Engineering– Rahman and Jaksa (Eds)
© 2022 Australian Geomechanics Society, Sydney, Australia, ISBN 978-0-9946261-4-1

Liquefaction characteristics of sand due to various irregular waves by cyclic torsional shear test

Caractéristiques de liquéfaction du sable dues à diverses vagues irrégulières par l'essai de cisaillement en torsion cyclique

Keisuke Ishikawa & Susumu Yasuda
Div. of Architectural, Civil and Environmental Engineering, Tokyo Denki University, Japan, ishikawa@g.dendai.ac.jp

Kousuke Oikawa
Architectural, Civil and Environmental Engineering, Graduate school of Tokyo Denki University, Japan

ABSTRACT: In this study, cyclic torsional shear tests were performed using various irregular waves to evaluate the liquefaction pr operties. Conventional stress methods and cumulative dissipation energy were deployed to analyze the effect of waveforms and dur ation on the liquefaction strength and properties. In the liquefaction test carried out using irregular waves, excess pore press ure is generated when the shear stress is approximately 0.6 times the maximum shear stress ratio. Shear strain occurs o nly when shear stresses of 0.3–0.4 times the maximum shear stress ratio are applied after the effective stress is lost. Th e increase in shear strain is more pronounced for irregular waves that are loaded repeatedly. The cumulative dissipation energy is a quantitative indicator of the ease of liquefaction due to the shapes of irregular waves. The ease of liquefacti on is more likely to be caused by the waveforms that are subjected to interaction of duration and strong shear stress co mpared to the sine wave.

RÉSUMÉ : Dans cette étude, des tests de cisaillement de torsion cyclique ont été réalisés en utilisant diverses ondes irrégulières pour évaluer les propriétés de liquéfaction. Des méthodes de contrainte conventionnelles et de l'énergie de dissipation cumulative ont été déployées pour analyser l'effet des formes d'onde et de la durée sur la force et les propriétés de liquéfaction. Dans le test de liquéfaction réalisé à l'aide d'ondes irrégulières, une pression interstitielle excessive est générée lorsque la contrainte de cisaillement est d'environ 0,6 fois le rapport de contrainte de cisaillement maximum. La déformation de cisaillement se produit uniquement lorsque des contraintes de cisaillement de 0,3 à 0,4 fois le rapport de contrainte de cisaillement maximal sont appliquées après la perte de la contrainte effective. L'augmentation de la déformation de cisaillement est plus prononcée pour les ondes irrégulières chargées de manière répétée. L'énergie de dissipation cumulée est un indicateur quantitatif de la facilité de liquéfaction due aux formes d'ondes irrégulières. La facilité de liquéfaction est plus susceptible d'être causée par les formes d'onde qui sont soumises à une interaction de durée et à une forte contrainte de cisaillement par rapport à l'onde sinusoïdale.

KEYWORDS: irregular wave, duration, liquefaction strength, dissipation energy, cyclic torsional shear test

1 INTRODUCTION

The 2011 Great East Japan and 2016 Kumamoto earthquakes have caused ground disasters in Japan owing to liquefaction. The former was a large trench-type earthquake, i.e., the duration of principal motions was extremely long. The latter was an inland earthquake, i.e., severe earthquakes with a maximum ground acceleration exceeding 1 G occurred several times. There are concerns that earthquakes similar to the Great Kanto earthquake and Tokyo Bay Northern earthquakes will occur in Tokyo. In the case of strong earthquakes expected to occur in the future, the effects of ground motion must be appropriately considered to predict liquefaction for trench-type and inland earthquakes.

For example, in liquefaction prediction via road bridge specification, the correction factors for seismic characteristics are set for trench-type and inland earthquakes. However, the correction factor for trench-type earthquakes is constant at C_w = 1.0, and the effects of waveform and duration are not considered in detail, as shown in Figure 1. These correction coefficients were devised by Iwasaki et al. (1978) and were determined by multiplying them by five coefficients from C_1 to C_5. Ishihara and Yasuda (1972) found experimentally that C_2 is the correction factor for irregularities in seismic motions and determined values of 1/0.55 to 1/0.70 for relatively loose sand. The average of the experimental values (1/0.65) has been adopted in the specifications for road bridges. Afterwards, Kokusho et al. (1981) and Tatsuoka et al. (1986) conducted similar experiments on dense and sand with a wide specimen density, respectively, and the correction factor was found to vary greatly with specimen density. These previous studies have obtained a duration of seismic motions of only a few tens of seconds, which is shorter than that of the Great East Japan earthquake. Mikami et al. (1997) carried out a study using the records of the 1995 Hyogo-ken Nanbu and the 1993 Kushiro-oki earthquakes for both shock and vibration types. They obtained results similar to those of Ishihara and Yasuda for loose sand but observed a decrease $1/C_2$ in duration as the density of the specimen increased. In addition, the authors conducted similar experiments at K-NET Urayasu during the Great East Japan earthquake and showed that the correction factor C_2 differs depending on the specimen density and fine grain content. It was also found that C_2 is particularly sensitive to long duration ground motions for dense specimens. Although there has been research focusing on the correction factor C_2, few studies have used the accumulated dissipation energy of the stress-strain relationship during liquefaction tests by irregular waves.

In this study, cyclic torsional shear tests were performed using various irregular waves to evaluate the liquefaction properties. Conventional stress methods and cumulative dissipation energy were deployed to analyze the effect of waveforms and duration on the liquefaction strength and properties.

2 TEST PROCEDURE

Cyclic torsional shear tests were performed. Hollow cylinders were used as specimens. The outer diameter, inner diameter, and height of the specimens were 100 mm, 60 mm, and 100 mm, respectively. The sample was Toyoura sand without fine grains. The soil particle density was $\rho_s = 2.650$ g/cm^3, and the maximum and minimum void ratios were 0.973 and 0.604, respectively. Each specimen was prepared by utilizing the air-pluviation method, and the relative density was adjusted to 70%. This was based on the previous studies conducted by the authors (Ishikawa et al. (2014)) and others (Ishihara and Yasuda (1972), Kokusho et al. (1981) and Tatsuoka et al. (1986)), which show that the specimen density is strongly affected by irregular waves. This study focused on the effect of irregular waveforms on medium-density specimens, which are more susceptible to irregular waves.

After the specimens were prepared, saturation was checked based on pore pressure coefficient B using CO_2 and deaerated water. The value of B was confirmed to be more than 0.95. Then, the specimens were consolidated under isotropic stress at an effective confining pressure (σ'_c) of 50 kN/m^2 or 100 kN/m^2 and a back pressure of 200 kN/m^2. Cyclic shear tests were conducted under stress control in undrained conditions after consolidation was completed.

The shape of the shear stress waveforms of the specimens were selected from the trench-type seismic motions observed at K-NET Urayasu and K-NET Haramachi during the Great East Japan earthquake and the Taisho-Kanto earthquake wave simulated by the Tokyo Metropolitan Government Bureau of Port and Harbor. In addition, the KiK-net Mashiki surface observation records of the 2016 Kumamoto earthquake and Northern Tokyo Bay earthquake provided by the Central Disaster Prevention Council of the Cabinet Office were selected as the inland earthquakes. The K-NET Urayasu wave is composed of a main shock and aftershocks 30 min after the main shock. The KiK-net Mashiki wave is composed of a foreshock, a main shock, and a combined foreshock and main shock. The waveforms of each earthquake are shown in Figure 1.

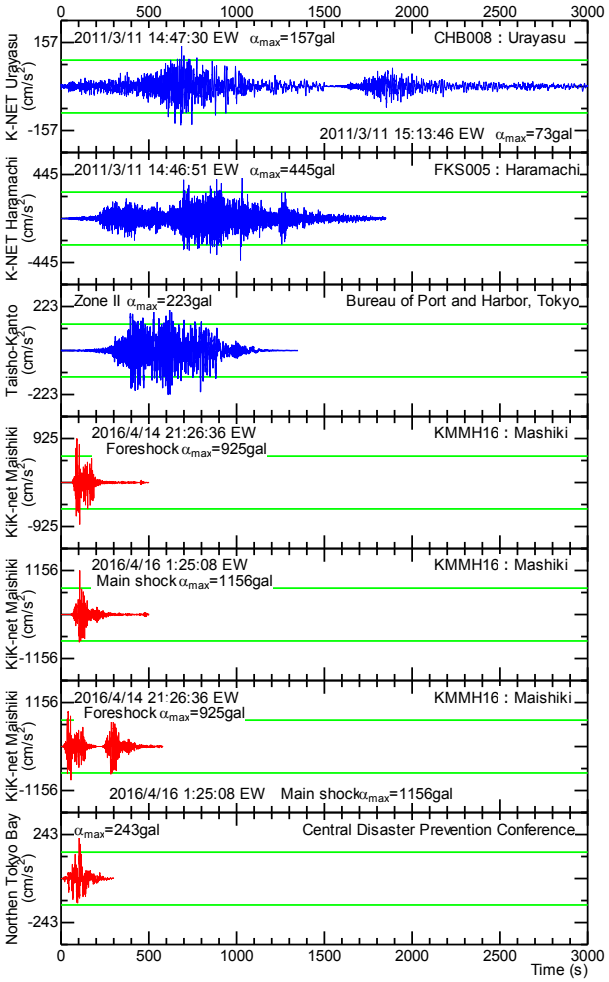

Figure 1. Irregular waves used in the cyclic torsional shear test

In sine wave loading, a uniform stress amplitude load with a loading speed of 0.1 Hz was applied until the excess pore pressure ratio ($\Delta U/\sigma'_c$) reached the effective confining pressure. Furthermore, irregular waves were applied by stretching the time axis of each irregular waveform shown in Figure 1 by a factor of 10. This is to ensure the reproducibility of the waveform in the air-pressure-controlled cyclic torsional shear test. The green line indicates the position where acceleration was 0.6 times the maximum acceleration, which was characterized by more than 10 and less than 10 shear cycles in the trench-type and inland earthquakes, respectively. The liquefaction strength ratios of the sine and irregular wave loads were determined through several tests, in which the amplitude of the sine and irregular wave loads was varied in stages while maintaining the waveform shape. Regarding the substitution of shear stress for the observed seismic wave shape, it was assumed that the shape of the cyclic shear stress waveform applied to the liquefied layer during an earthquake was similar to the acceleration at the ground surface.

3 TEST RESULTS

3.1 *Liquefaction behavior under irregular wave loading*

Figures 2 and 3 show the representative examples of the results of the cyclic shear tests performed using irregular waves in which liquefaction is reached. Figure 2 shows the test results for the trench-type earthquakes with a large number of shear cycles, and Figure 3 shows the test results for the inland-type earthquakes with a small number of shear cycles.

Figure 2 shows that the excess pore water pressure starts to rise at approximately 60% of the maximum shear stress and reaches the effective confining pressure close to the maximum shear stress. Shear strain increases when the excess pore pressure reaches the effective confining pressure and effective stress is lost. In the case of a waveform that reproduces the aftershocks of 1500 s, such as the K-NET Urayasu wave, large strains are generated even though the input shear stress is approximately half of that of the main shock wave. The same amount of shear stress is applied after the maximum shear stress in the K-NET Haramachi and Taisho-Kanto waves. A large shear strain is generated in this process, similar to the behavior of the K-NET Urayasu wave aftershocks.

Figure 3 shows that the duration of seismic motions is short and the number of acting repetitive shears is less for inland-type seismic waves compared to trench-type seismic waves. This indicates that the input shear stress amplitude of the inland-type seismic waves is larger than that of the trench-type seismic waves. Similar to the results for the trench-type earthquakes, the excess pore pressure starts to rise at approximately 60% of the maximum shear stress and rises sharply close to the maximum shear stress. Then, the effective confining pressure is reached after several waves of maximum shear stress. The increase in shear strain is similar to that for the trench-type seismic waves. However, shear strain dose not increase significantly after the maximum shear stress because the increase is only a few large shear stress waves after the maximum shear stress is applied.

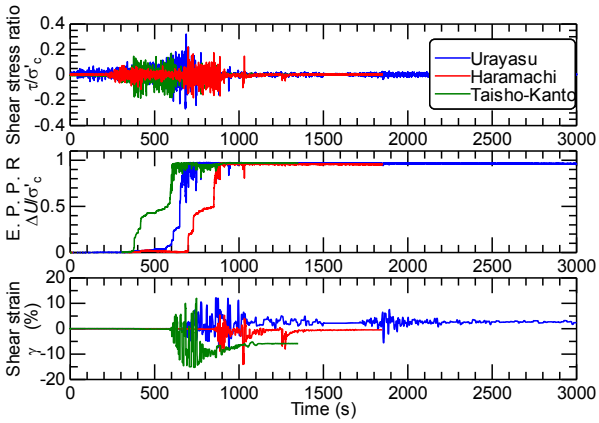

Figure 2. Results of liquefaction test for trench-type waves

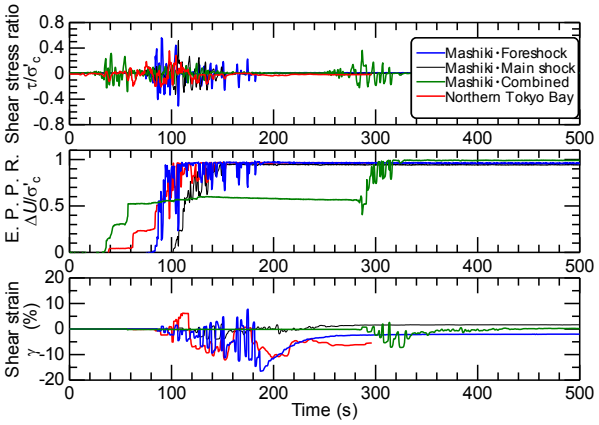

Figure 3. Results of liquefaction test for inland-type waves

3.2 *Comparison of liquefaction strength ratios based on stress method*

The liquefaction strength ratio is determined using the approach developed by Ishihara and Yasuda, and it is defined as follows:

1) Based on the excess pore pressure ratio: The excess pore pressure ratio is defined as the residual excess pore pressure ratio (U_r/σ'_c) at the end of the irregular wave loading. The shear stress amplitude is represented by the maximum shear stress ratio (τ_{max}/σ'_c) over time of the shear stress amplitude applied at this time. Based on the relationship between the maximum shear stress ratio and residual excess pore pressure ratio, the liquefaction strength ratio ($\tau_{max,l,U}/\sigma'_c$) is the maximum shear stress ratio at $U_r/\sigma'_c = 0.95$.
2) Based on shear strain: The maximum double amplitude shear strain (γ_{DAmax}) is arranged on the horizontal axis and the maximum shear stress ratio on the vertical axis. The liquefaction strength ratio ($\tau_{max,l,\gamma}/\sigma'_c$) is the maximum shear stress ratio at a double amplitude maximum shear strain of 7.5%.
3) Based on the relationship between the excess pore pressure ratio and cyclic shear stress ratio at 20 cycles: In the case of sine wave loading, the liquefaction strength ratio ($\tau_{d,l,U}/\sigma'_c$) is the shear stress ratio at $\Delta U/\sigma'_c = 0.95$.
4) Based on the relationship between the shear stress ratio and the double amplitude shear strain at 20 cycles: The liquefaction strength ratio ($\tau_{d,l,\gamma}/\sigma'_c$) is the shear stress ratio at γ_{DA} =7.5%.

Figure 4 shows the liquefaction strength ratio based on the residual pore pressure ratio and excess pore pressure ratio, and Figure 5 shows the liquefaction strength ratio based on the

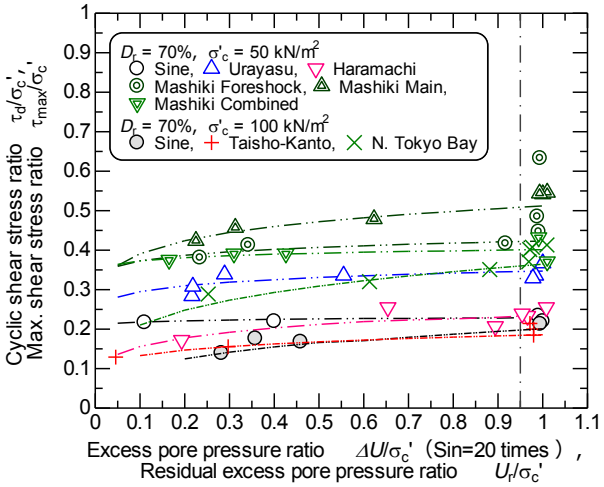

Figure 4. Liquefaction strength curve based on excess pore pressure

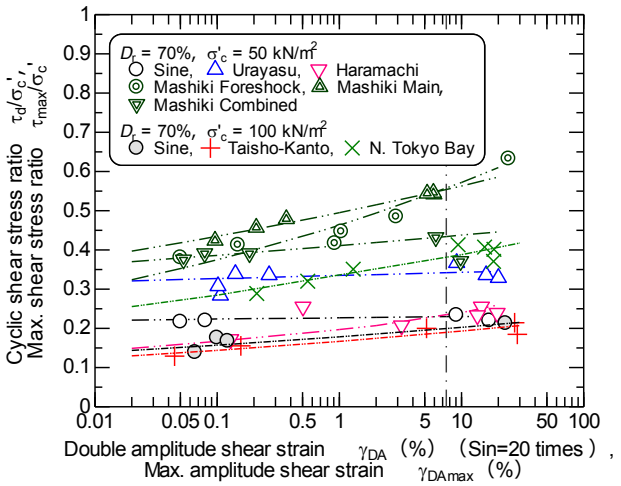

Figure 5. Liquefaction strength curve based on shear strain

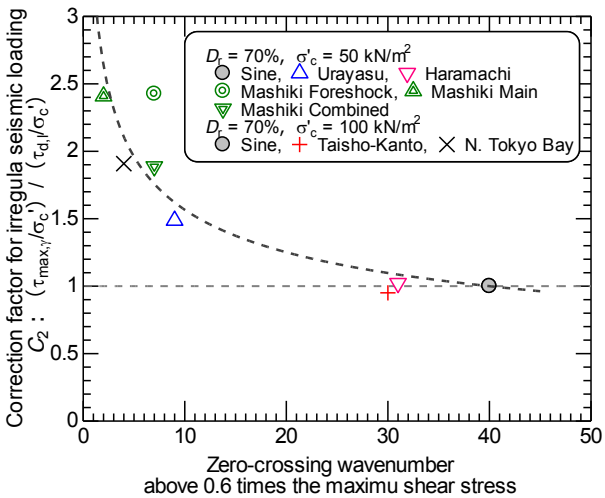

Figure 6. Relationship between zero-crossing wavenumber and correction factor C_2

maximum double amplitude shear strain and double amplitude shear strain. Figure 4 shows that the shear stress ratio at an excess pore pressure ratio of 0.95 differs depending on the shape of the irregular waves. The liquefaction strength ratios are lowest for the sine wave, K-NET Haramachi wave, and Taisho-Kanto

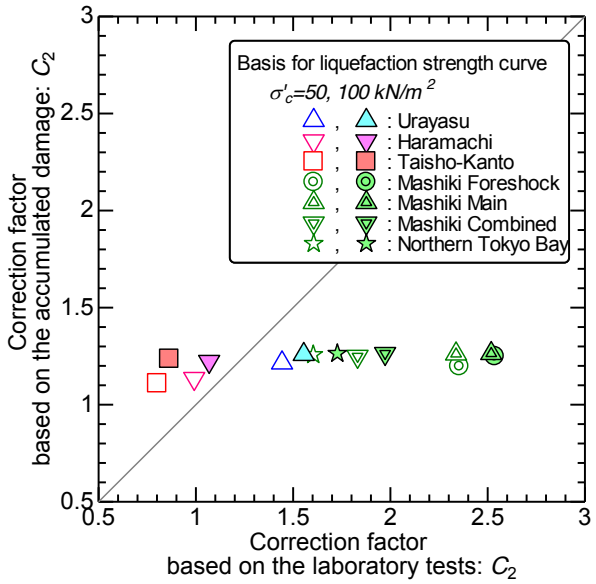

Figure 7. Correction factors based on accumulated damage and laboratory tests

earthquake wave, followed by the K-NET Urayasu wave. For the Kumamoto earthquake, the Northern Tokyo Bay earthquake wave is smaller than the KiK-net Mashiki wave. The shear stress ratio at a double amplitude shear strain of 7.5% is similar in Figures 4 and 5. The slope of the liquefaction strength curve for the inland-type irregular waves is larger than that for the sine wave. This is considered to be related to the duration of the irregular waves. Moreover, for shear strain to occur, the shear stress must be 0.3–0.4 times the maximum shear stress of the input waveform after the excess pore pressure almost reaches the effective confining pressure. Therefore, the liquefaction strength ratios based on the excess pore pressure and shear strain are larger for the inland-type earthquakes, which have a shorter duration, compared to the trench-type earthquakes.

Figure 6 shows the relationship between the zero-crossing wavenumber above 60% of the maximum shear stress for each irregular wave and the correction factor for irregular seismic loading (C_2). C_2 is the ratio between the liquefaction strength ratios for the irregular waves and sine wave. The liquefaction strength ratio is defined based on shear strain. C_2 is 2.0–2.4 for the KiK-net Mashiki and Northern Tokyo Bay waves, which have the lowest number of repetitions at more than 60% of the maximum shear stress. In contrast, C2 is approximately 1.0 for the K-NET Haramachi and Taisho-Kanto waves, which have the highest number of repetitions.

3.3 *Comparison of correction factors based on accumulated damage and laboratory tests*

The correction factor is calculated using accumulated damage by decomposing the time history of acceleration shown in Figure 1 into half waves and extracting the maximum acceleration of each half wave. Then, the number of cycles corresponding to the maximum acceleration at each half wave is calculated using the liquefaction strength curve (σ'_c = 50 kN/m^2 and 100 kN/m^2) with sine loading. Accumulated damage is calculated using the following equation:

$$D = \sum\{1/(2 \times N_c)\} \quad (1)$$

N_C is the number of cycles corresponding to the maximum acceleration at each half wave. Based on the above equation, liquefaction is assumed to occur when D = 1.0. The amplitude of the maximum acceleration at each half wave is adjusted. The maximum acceleration obtained in this manner is the maximum shear stress calculated from accumulated damage. C_2 is determined from the ratio of the maximum shear stress to the liquefaction strength ratio for the sine wave.

Figure 7 compares the correction factors obtained using laboratory tests and accumulated damage. The correction factors for accumulated damage are in a range of 1.1–1.3, and they do not vary significantly with the shape of the waveform. The correction factor for accumulated damage is underestimated for the short-duration inland-type earthquakes and overestimated for the long-duration trench-type earthquakes. When the relative density of Toyoura sand is 70%, the slope of the liquefaction strength curve is loose. In other words, the change in the shear stress ratio with respect to the cyclic number is small. Thus, the shape of the waveform negligibly affects accumulated damage.

3.4 *Comparison of liquefaction characteristics based on cumulative dissipation energy*

Numerous previous studies (e.g., Kokusho, (2013)) have proposed the evaluation of liquefaction behavior using the dissipation energy during the liquefaction process. The cumulative dissipation energy is calculated based on the relationship between the shear stress and shear strain of each irregular wave. Additionally, the effect of the shape of each irregular waveform on the energy characteristics of the liquefaction process is evaluated. The cumulative dissipation energy is calculated by obtaining the area of the hysteresis curve from the shear stress–shear strain relationship.

$$\sum \Delta W = \int \tau \, d\gamma \quad (2)$$

The normalized cumulative dissipation energy ($\Sigma\Delta W/\sigma'_c$) is defined as the cumulative dissipation energy divided by the initial confining pressure.

The relationship between the normalized cumulative dissipation energy and excess pore pressure ratio for the sine wave and irregular waves is shown in Figure 8. The results for the trench-type and inland-type waves are shown separately. The initial liquefaction for the sine wave at $\Sigma\Delta W/\sigma'_c$ = 0.01 and $\Delta U/\sigma'_c$ = 1.0 is independent of the effective confining pressure, and there is negligible difference between the curves for different types of waves. For the K-NET Urayasu wave, the normalized cumulative dissipation energy required to reach the initial liquefaction is the same as that for the sine wave. In contrast, for the K-NET Haramachi and Taisho-Kanto waves, the normalized cumulative dissipation energy required to reach the initial liquefaction is 1/5–1/2 of that for the sine wave. This suggests that the shape of the trench-type earthquake waveforms can easily cause liquefaction; this can be quantitatively explained using energy. In contrast, for the inland-type earthquake waveforms, the normalized cumulative dissipation energy required to reach the initial liquefaction is smaller and the initial liquefaction requires approximately the same time as that for the sine wave.

The relationship between the normalized cumulative dissipation energy and shear strain for the sine wave and irregular waves is shown in Figure 9. In the case of the sine wave, complete liquefaction (γ_{DA} =7.5%) is reached at $\Sigma\Delta W/\sigma'_c$ = 0.015–0.020 regardless of the effective confining pressure. For the K-NET Urayasu wave, the normalized cumulative dissipation energy required for complete liquefaction is almost equal to or slightly larger than that for the sine wave. However, for the K-NET Haramachi and Taisho-Kanto waves, the normalized cumulative dissipation energy required for complete liquefaction is approximately half of that for the sine wave. The maximum shear strains differ depending on the shape of the irregular waves, for the same normalized cumulative dissipation energy. This quantitatively explains why the K-NET Haramachi and Taisho-Kanto waves, which have a large number of repetitions, are more likely to cause liquefaction. In contrast to the trench-type waves,

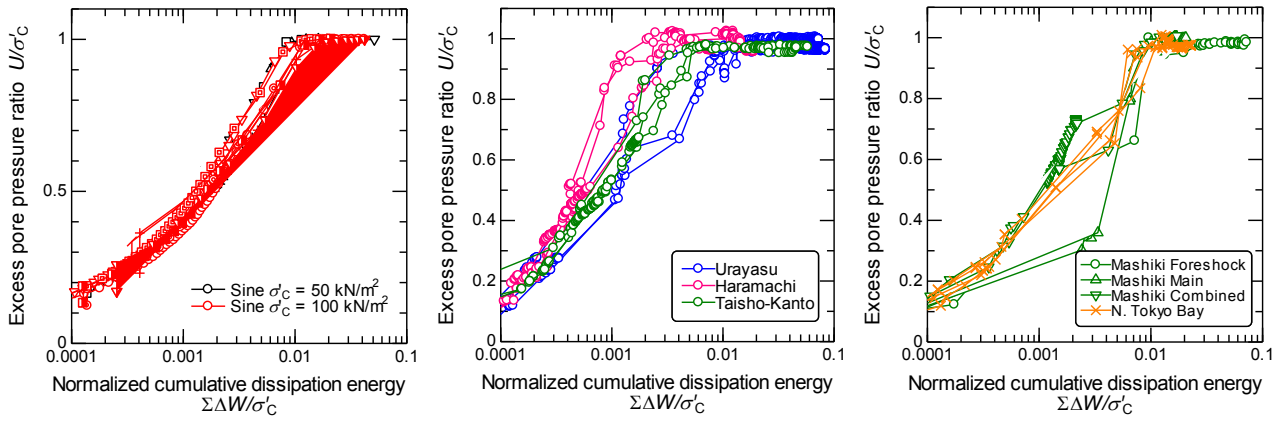

Figure 8. Relationship between normalized cumulative dissipation energy and excess pore pressure ratio

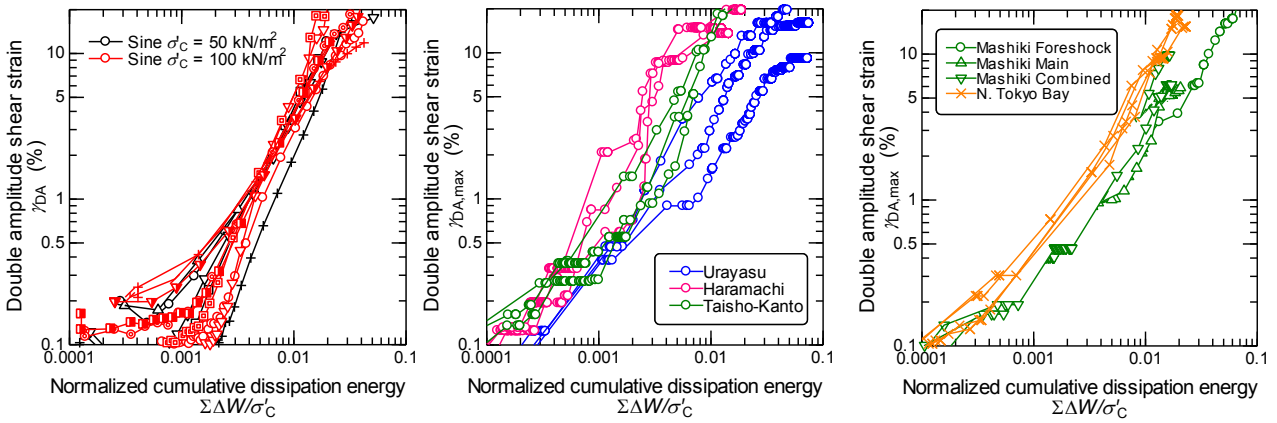

Figure 9. Relationship between normalized cumulative dissipation energy and double amplitude shear strain

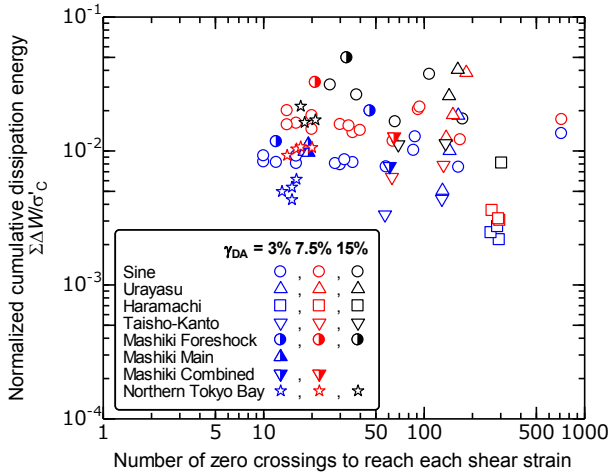

Figure 10. Relationship between the number of zero crossings and normalized cumulative dissipation energy

the inland-type waves have a small number of loading cycles. For the KiK-net Mashiki foreshock wave, which has the lowest number of cycles, the normalized cumulative dissipation energy required for complete liquefaction is approximately 1.5 times larger than that for the sine wave.

Figure 10 shows the relationship between the normalized cumulative dissipation energy and the number of zero crossings ($\tau_{max}/\sigma'_c \times 0.1$) for different shear strains (γ_{DA} = 3.0%, 7.5%, 15%) and all irregular waves. At a shear strain of less than 7.5%, the cumulative dissipation energy of the sine wave differs; however, it increases gradually and slightly with the number of cycles. On the contrary, at a shear strain of 7.5%, the cumulative dissipation energy required for reaching complete liquefaction for the K-NET Haramachi and Taisho-Kanto waves, which have a large number of cycles, is lower. In addition, the cumulative dissipation energy of the K-NET Urayasu wave differs by a factor of three depending on whether there is a main shock or an aftershock at the time of complete liquefaction. The cumulative dissipation energy required for complete liquefaction for the irregular waves decreases as the number of cycles increases. Additionally, the cumulative dissipation energy required for complete liquefaction for long-duration seismic waves is different by approximately one order of magnitude.

4 CONCLUSIONS

The effects of waveform shape and duration on liquefaction strength and behavior were experimentally evaluated by performing cyclic torsional shear tests using irregular waves with various shapes.

In the liquefaction test carried out using irregular waves, excess pore pressure is generated when the shear stress is approximately 0.6 times the maximum shear stress ratio. Shear strain occurs only when shear stresses that are 0.3–0.4 times the maximum shear stress ratio are applied after the effective stress is lost. The increase in shear strain is more pronounced for the irregular waves that are loaded repeatedly.

The correction factor for irregular seismic loading is correlated with the number of cycles when approximately 0.6 times the maximum shear stress ratio is applied.

The cumulative dissipation energy is a quantitative indicator of the ease of liquefaction due to the shapes of irregular waves. The ease of liquefaction is more likely to be caused by the waveforms that are subjected to interaction of duration and strong shear stress compared to the sine wave.

5 ACKNOWLEDGEMENTS

This work was supported by JSPS KAKENHI Grant Number 19K15091. The date of K-NET and KiK-net of NIED are used for the observed seismic waveforms. The laboratory tests were conducted in cooperation with graduates of Tokyo Denki University.

6 REFERENCES

Association for Promotion of infrastructure Geospatial Information Distribution. 2019. https://www.geospatial.jp/gp_front/

Bureau of Port and Harbor, Tokyo Metropolitan Government. 2019. https://www.kouwan.metro.tokyo.lg.jp/business/l2.html

Ishihara K. and Yasuda S. 1972. Sand Liquefaction due to irregular excitation. *Soils and Foundations* 12 (4), 65-78.

Ishikawa K., Yasuda S., and Aoyagi T. 2014. Studies on the reasonable liquefaction-prediction method of the 2011 Great East Japan Earthquake. *Japanese Geotechnical Journal* 9 (2), 169-183. in Japanese.

Iwasaki T., Tatsuoka F., Tokida K. and Yasuda S. 1978. A practical method for assessing soil liquefaction potential based on case studies at various sites in Japan. *5th Japan Earthquake Engineering Symposium*, 641-648. in Japanese.

Kokusho T., Shimada M. and Kato S. 1981. Characteristics of dense sand cyclicly sheared under undrained condition. *Proc. of the 16th Japan National Conf. on SMFE*, 609-612.

Kokusho T. 2013. Liquefaction potential evaluations: Energy-based method versus stress-based method. *Canadian Geotechnical Jo urnal* 50 (10), 1088-1099.

Mikami T., Sako S., Hatakeyama M. and Furuta I. 1997. Experim ental study on liquefaction characteristics attended to earthqua ke wave form. *Annual technical report of OYO Corporation S pecial issue on 1995 Hyogoken-Nanbu earthquake*. 237-255. in Japanese.

National Research Institute for Earth Science and Disaster Resilien ce. 2019. *K-NET, KiK-net, National Research Institute for Ear th Science and Disaster Resilience*, https://doi.org/10.17598/NI ED.0004

Tatsuoka F., Maeda S., Ochi K. and Fujii S. 1986. Prediction of cyclic undrained strength of sand subjected to irregular loading. *Soils and Foundations* 26 (2), 73-90.